Acta Geologica Sinica (English Edition), 2023, 97(2): 662–680

Mapping Structurally Controlled Alterations Sparked by Hydrothermal Activity in the Fatira–Abu Zawal Area, Eastern Desert, Egypt

Mohamed BADAWI[1, 2, *], Mahmoud ABDELATIF[3], Ali SHEBL[4, 5], Farid MAKROUM[2], Ahmed SHALABY[2] and Norbert NÉMETH[1]

[1] *Institute of Exploration Geosciences, University of Miskolc, Miskolc 3515, Hungary*
[2] *Department of Geology, Mansoura University, Mansoura 35516, Egypt*
[3] *Department of Geology, South Valley University, Qena 83523, Egypt*
[4] *Department of Mineralogy and Geology, University of Debrecen, Debrecen 4032, Hungary*
[5] *Department of Geology, Tanta University, Tanta 31527, Egypt*

Abstract: The Eastern Desert of Egypt suffered a protracted period of deformation triggered by cratonization of the new juvenile crust known as the Arabian Nubian Shield (ANS), which has been proposed for potential gold discoveries associated with the corresponding tectonic event. The Fatira area, on the border of Egypt's Northern and Central Eastern Deserts, is covered with metavolcanic rocks twisted by a dextral relocation of the Fatira Shear Zone (FSZ) relative to the Barud magmatic body. The recent study evaluated many deformed post-orogenic granitic intrusions and felsite dikes associated with promising mineralization localities, notably orogenic gold deposits. The combination of various field observations and remote sensing data, followed by the analysis of aeromagnetic enhanced maps, allowed the differentiation of distinct lithologies, structural features, and hydrothermal alterations in the study area. Additionally, the integrated results obtained from the different interpretation techniques are utilized to identify and confirm the previously supposed mineralized localities in the Fatira and Abu Zawal areas and predict other matched localities. The final ASTER, Sentinel 2 hydrothermal alteration, and orientation entropy heat maps demonstrate the association between these mineralized regions and major structures related to the FSZ late stage of deformation rather than other structures studied throughout the area of interest.

Key words: gold, granite, island arc association, Pan-African Orogeny, Egypt

Citation: Badawi et al., 2023. Mapping Structurally Controlled Alterations Sparked by Hydrothermal Activity in the Fatira–Abu Zawal Area, Eastern Desert, Egypt. Acta Geologica Sinica (English Edition), 97(2): 662–680. DOI: 10.1111/1755-6724.15019

1 Introduction

The Eastern Desert of Egypt is highly prospective for potential gold deposits that occur as shear zone-hosted, disseminated sulfide mineralization or as quartz-carbonate veins along major structures in ophiolitic and island arc terranes (Zoheir, 2011). A wide variety of rock types, including gabbroic and granitoid rocks, are possible hosts for gold mineralization, particularly sheared post-orogenic granites that cut through ophiolitic rocks and molasse-type deposits (El Gaby et al., 1988; Hussein, 1990; Murr, 1999; Harraz, 2002; Klemm and Klemm, 2013). One of the primary controls on such mineralization is the spatial association with the major transpressional and transtensional structures (Helmy et al., 2004; Zoheir and Akawy, 2010; Zoheir, 2011; Klemm and Klemm, 2013).

Several authors (e.g., Hume, 1934; Sabet et al., 1972; Akaad et al., 1973; Botros, 1991; Haroun, 2001; Abd El Monsef et al., 2020) previously conducted extensive exploration in the Fatira-Abu Zawal region for various purposes, either for lithological mapping or determining the genetic relationship between gold mineralization and specific lithologies (i.e., intrusive granites and auriferous felsite dykes). However, gold mineralization types are still disputed; a considerable number of gold deposits previously categorized as orogenic have been reclassified as intrusion-related in recent years (Klemm et al., 2001; Botros, 2004; Surour et al., 1999; Abd El Monsef et al., 2018). Abd El Monsef et al. (2020) confined the Fatira gold lode to altered felsite dykes, large quartz veins cutting through host granitic rocks, and a siliceous shear zone. This type of deposit is typically represented at the Fatira gold mine, which is hosted within two distinct blocks of metavolcanics and granodiorites separated by a significant shear zone. Fatira gold mine is one of the most well-known gold deposits in Egypt's Northern Eastern Desert, dating back to the Pharaonic New Kingdom and Roman periods (Abd El Monsef et al., 2020). Throughout the previous century, mine work production was largely intermittent and limited to shallow pits along sub-parallel felsic dykes. Reevaluation of gold deposits by the Egyptian Geological Survey between 1975 and 1977 and later by Alexander Nubia International Inc. attained a

* Corresponding author. E-mail: mohamedabdelhadi@mans.edu.eg

http://www.geojournals.cn/dzxbcn/ch/index.aspx; https://onlinelibrary.wiley.com/journal/17556724

mean gold content of 2.2 g/t and 2.6 g/t, respectively (Abd El-Nabi, 1977; Azzaz et al., 1997).

In recent years, the integration of remote sensing data and geophysical methods has achieved a considerable leap in defining criteria that serve as indicators for gold occurrences (Hasan et al., 2014; Eldosouky et al., 2017; Abdelkareem et al., 2018; Ghazala et al., 2021, Shebl et al., 2021). In this paper, we followed the same strategy by combining multisource datasets with field observations to (1) evaluate the geology of the Fatira-Abu Zawal area, (2) study the relationships between the juxtaposing rock units, particularly those related to mineralization, and (3) highlight the tectonic framework of the research region and its key features relevant to hydrothermal alteration assemblages accompanied by Au-mineralization, which could improve and provide vital information to estimate the probable mineralized areas for further exploration.

2 Geological Setting

2.1 Regional framework

The crystalline basement rocks exposed in the Eastern Desert and Sinai constitute the northern juvenile arc terrain of the Arabian–Nubian Shield (ANS), which was cratonized during the late Neoproterozoic Pan-African Orogeny (PAO) (900–550 Ma; Fig. 1a; Stern, 1994; Kusky et al., 2003). The evolutionary tectonic framework of the PAO was initiated by the closure of the Mozambique Ocean between the East and West Gondwana continental blocks. This closure resulted in the consolidation of many juvenile arc and back-arc igneous and sedimentary rock layers, with several terrane sutures indicated by mafic to ultramafic ophiolitic assemblages and fragments. Several gold occurrences have been discovered at the sheared edges of granitic intrusions or along contacts between different lithologies: sheared silica- and carbonate-altered ultramafic rocks along numerous fault zones. Orogenic gold formed following the cessation of arc-terrane accretion in the ANS and during a period when the majority of the shield became established, which transitioned from compressional/transpressional terrane accretion to post-amalgamation transtensional shearing. Within the newly formed shield, this was also defined by a petrogenetic change from pre- to syn-accretionary, arc-related calc-alkaline I-type magmatism to late or post-tectonic A-type magmatism. Concurrently, the Eastern Desert was impacted by a widespread crustal flow of aqueous fluids, especially on the vast strike-slip shears that were still active (Zoheir et al., 2019). The Eastern Desert, in particular, is dominated by a variety of lithologies, including gneisses and ophiolitic mélange that have been intruded by volcanics and syn-to-late orogenic granitoids, and are overlain by molasse-type sediments and lately intruded by post-tectonic granites and dike swarms (Ries et al., 1983, El Gaby et al., 1988, Stern et al., 2004).

Structurally, the Eastern Desert is divided into three main regions, namely, the Southern, Central, and Northern Eastern Deserts (SED, CED, NED), separated by two main structural shear zones: the WNW sinistral Kom Ombo–Houdin and the ENE dextral Qena–Safaga corridors, respectively (Fig. 1b, modified after Moussa et al., 2008). Moreover, smaller structural subdivisions were proposed based on differences in structural

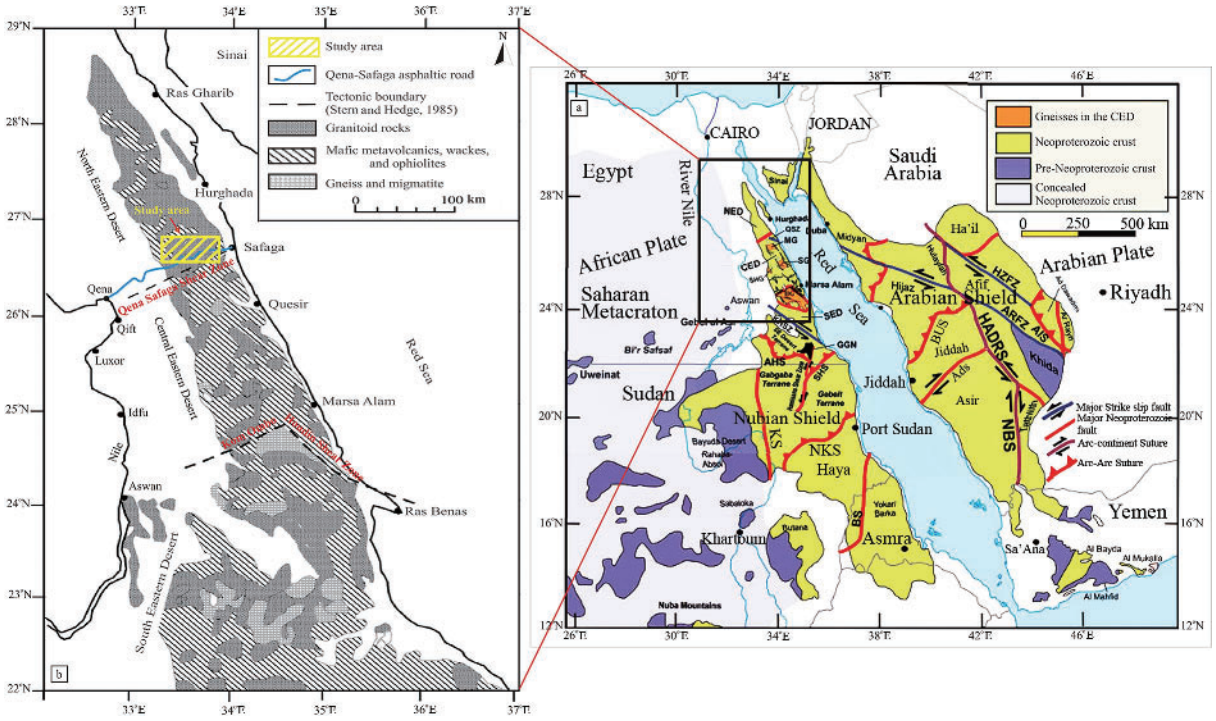

Fig. 1. (a) Simplified geological map of the Arabian–Nubian Shield with boundaries defined by sutures and/or strike-slip faults (red lines) adjacent to older continental crust after Johnson et al. (2011); (b) simplified geological map of the Eastern Desert of Egypt (modified after Moussa et al., 2008).

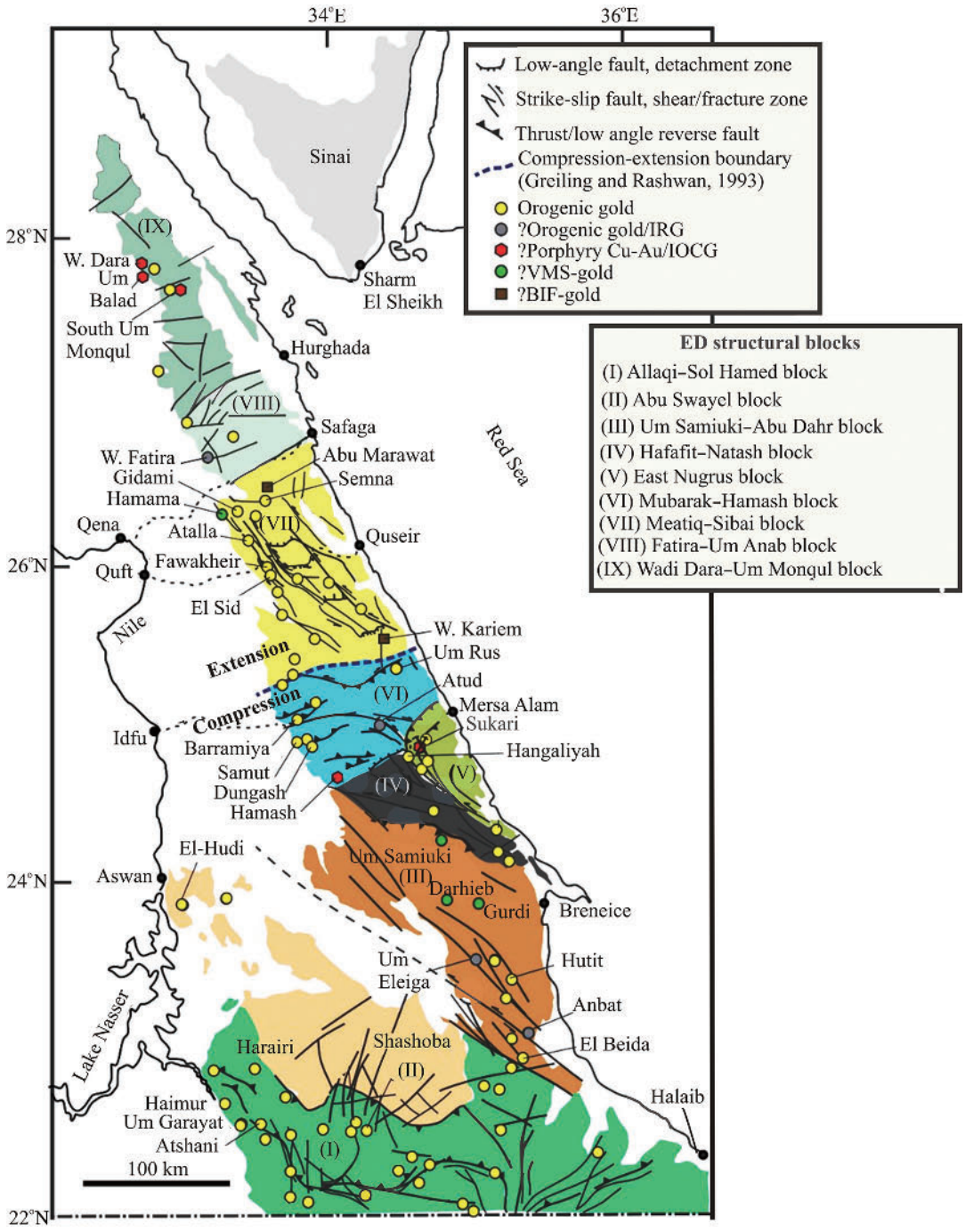

Fig. 2. Concentrations of gold occurrences in structural blocks of the ED of Egypt (Zoheir et al., 2019).

orientations, the abundance of gold occurrences, and concentrations of other ore types (Zoheir et al., 2019). Among these blocks are the Allaqi–Sol Hamed, Mubarak–Hamash; Meatiq–Sibai; and Fatira–Um Anab blocks (Fig. 2). The margins of these structural blocks are mostly defined by significant faults and shear zones, namely the steeply dipping NW sinistral strike-slip faults and their dextral ENE-trending conjugate faults (Greiling et al., 1988; Fritz et al., 1996; Loizenbauer et al., 2002; Helmy et al., 2004; Shalaby et al., 2005; Zoheir et al., 2017; Abu-Alam et al., 2018).

2.2 Geology of the study area

The area of Fatira is a part of the NED, extending parallel to the Qena–Safaga zone near Safaga city and can be accessed by the Qena–Safaga asphaltic road (Fig. 1b). It covers about 1800 km^2 and is dissected by many wadies, of which the most important ones are Wadi Fatira, Wadi Abu Zawal, and Wadi Barud, trending roughly NW, NW, and NE, respectively, between the mountainous peaks, Gebel Abu Elhasan, Gebel Abu Murra, Gebel Ras Barud, and Gebel Um Anab (Fig. 3).

Our fieldwork for the study area revealed the

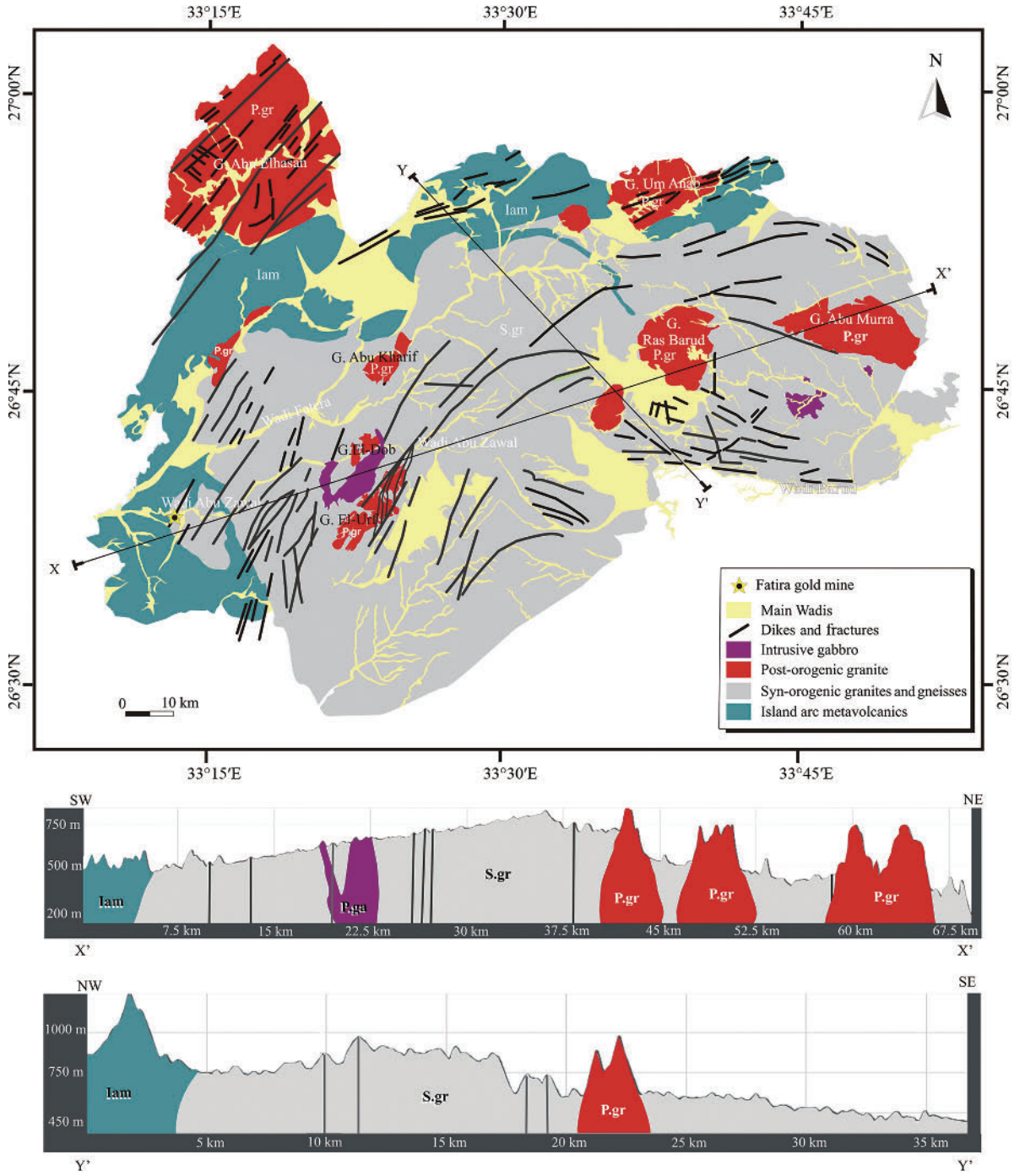

Fig. 3. (a) Geological map of the Fatira area, Eastern Desert, Egypt; (b) geological cross-sections xx' and yy' of the Fatira –Abu Zawal area (based on the automatic topographic profile generated by Google Earth).
Abbreviations: Iam = island arc metavolcanics; Sgr = syn-orogenic granodiorites; Pga = post-orogenic gabbros; Pgr = post-orogenic granites.

predominancy of many rock units, including the island arc metavolcanics, syn- to late-orogenic granodiorites, post-orogenic intrusives, and post-orogenic dikes (Fig. 3).

The island arc metavolcanics clipped off the northern and western portions of the mapped region at the Fatira and Abu Zawal areas, juxtaposing the syn-orogenic Barud granodiorites for approximately 45 km and 20 km, respectively (Fig. 3). These metavolcanics are mostly composed of weakly metamorphosed, heavily fractured, dark green, fine-grained andesitic rocks intercalated with minor metapyroclastics and the Algoma-type Banded Iron Formation (BIF), especially in the Abu Zawal area (Fig. 4a, b). The Fatira metavolcanics are exposed as highly sheared, nearly vertical sheets, which strike markedly concordant with the foliation of the discrete gneissic bands of the Barud batholith along the FSZ, oriented in the same direction (Fig. 4c). From the map view, the Fatira and Abu Zawal metavolcanics form a NE to ENE curve that gets

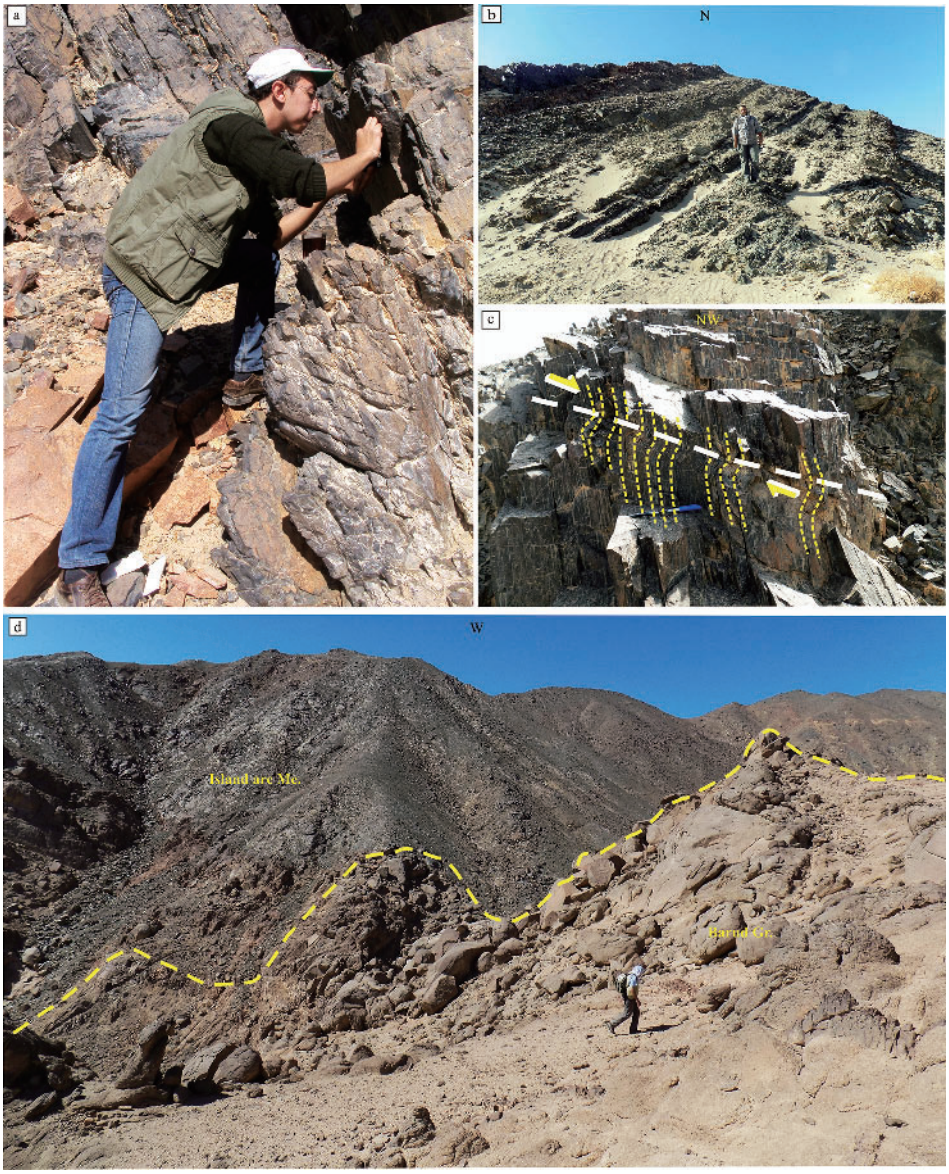

Fig. 4. Field photos showing: (a) Fatira low-grade metavolcanics; (b) BIF at Abu Zawal area; (c) vertical sheets of Fatira sheared metavolcanics; (d) intrusive contact of Barud syn-orogenic granodiorite with island arc metavolcanics.

narrower eastward, exhibiting a kinked thin tabular stripe of 20 km in length and half a km in width, which extends easterly in the NW–SE direction, where it is truncated by the Ras Barud post-orogenic granite (Fig. 3). These extrusive rocks are composed of plagioclase, hornblende, and quartz. Iron oxides, chlorite, and epidote are all accessory minerals (Fig. 6a).

The syn- to late-orogenic Barud granodiorites form an ellipsoidal belt that crosses traversely the Eastern Desert with a long axis trending roughly in the ENE–WSW direction (Fig. 3). Field observations of the Barud belt show that these granites are considerably weathered, forming moderate topographic slopes with intrusive features to the western Fatira and Abu Zawal sheared metavolcanics (Figs. 4d, 5a). However, these granodiorites have discrete gneissic bands, particularly on the outer rims of the magmatic body (Fig. 5b). The two geologic cross sections x–x' and y–y' across the area of study in the NE–SW and NW–SE directions show the convexity of the Barud granodioritic domal surface, proving the magmatic protolith that was intruded later by post-orogenic intrusives and dikes (Fig. 3). These rocks are predominantly composed of plagioclase, quartz, K-feldspars, hornblende, and biotite (Fig. 6b, c). Sericite, kaolinite, epidote, chlorite, calcite, and iron oxides represent the alteration phase, whereas zircon and sphene are typical accessory minerals.

The post-orogenic granites are pink-colored, coarse-to-medium-grained rocks that range in composition from syenogranites to monzogranites (Figs. 3, 5c). This unit is characterized by sharp contacts with the island metavolcanics and Barud syn- to late-orogenic granodiorite rocks. These granites are mainly represented by many mountainous peaks; Gebel Ras Barud, Gabal El-

Fig. 5. Field photos showing: (a) Barud syn-orogenic granodiorite; (b) Barud banded gneiss; (c) sheared post-orogenic granites of Abu Zawal area, (d) intrusive post-orogenic gabbros; (e, f) post orogenic basic and acidic dike series crosscutting Barud granodiorites; (g) Fatira gold mine at Abu Zawal area.

Urf, Gebel Abu Murra, Gabal El-Dob, Gabal Um Anab, and Gabal Abu Kharif granites. They form heavily sheared oval to elongate plutons extending in the NE-SW directions, concordant with the major NE-trending faults (Figs. 3, 5c). The majority of their composition is quartz, biotite, plagioclase, orthoclase, and microcline (Fig. 6e). The alteration phases include kaolinite, epidote, sericite, iron oxides, and calcite.

The post-orogenic gabbros at Wadi Abu Zawal and Barud are of low to moderate relief and occur as small rounded or elongated bodies, intruding the Barud granodioritic rocks (Figs. 3, 5d). They are hard, massive, and very coarse-grained of greenish black in color (Fig. 6f). They consist of plagioclase and augite. Plagioclase crystals are partly or completely embedded in large augite crystals, forming subophitic and ophitic textures, respectively.

The post-orogenic dikes of the area cross the Barud granodiorites, which are categorized mostly by two series of basic and acidic dikes reflecting multiple magmatic

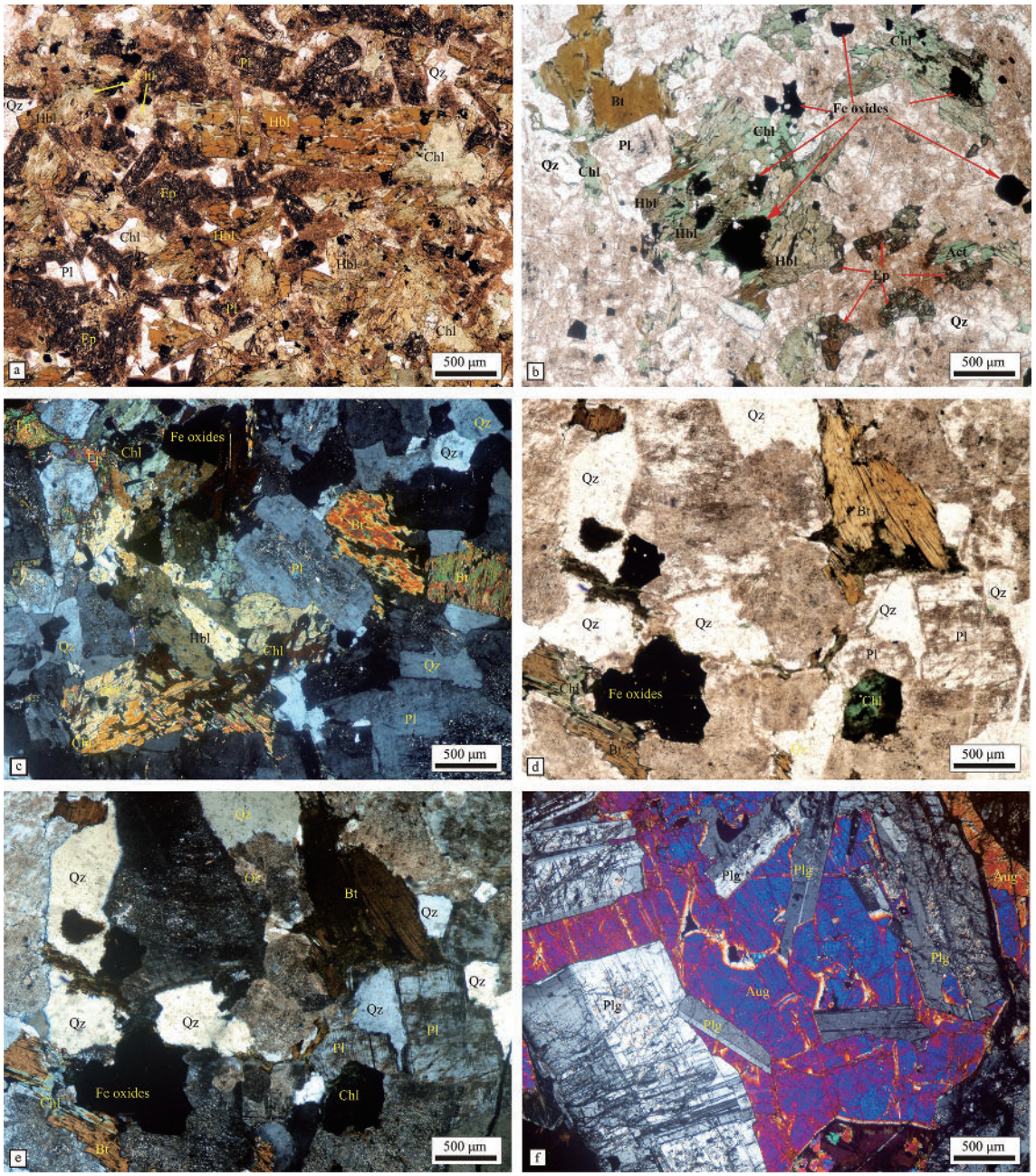

Fig. 6. Thin-section photomicrographs of the lithologies of Fatira area showing: (a) porphyritic texture of plagioclase and hornblende phenocrysts in meta-andesites (ppl); (b, c) heavily altered granodiorite (ppl and xN); (d, e) heavily altered monzogranite (ppl and xN); (f) augite crystals enclose plagioclase laths forming sub-ophitic textures in post-orogenic gabbro (xN).
Abbreviations: Qz–quartz; Pl–plagioclase; Hbl–hornblende; Bt–biotite; Chl–chlorite; Ep–epidote; Or–orthoclase; Aug–augite; Act–actinolite.

phases (Figs. 3, 5e, f). In comparison to the host rocks, the acidic dykes are more resistant to weathering. As a result, they produce prominent ridges and spines. These dykes are particularly conspicuous in the NE–SW and E–W directions at Abu Zawal and Barud, respectively. Several gold occurrences in the Wadi Fatira and Abu Zawal areas are hosted by volcanic and subvolcanic rocks, NE-trending felsic dike swarms, and quartz veins associated with hydrothermal alteration (Murr, 1999; Klemm and Klemm, 2013). These altered felsite dikes form a set of several parallel to subparallel, gently dipping and highly dull, reddish to yellowish altered bodies near the granitic body (Figs. 3, 5g). Such extensive intrusions of post-orogenic granites and associated felsic dikes into granodiorite rocks are favorable for gold deposits, which are ideally exemplified by the Fatira gold mine (Abu-Alam et al., 2019).

3 Materials and Methods

3.1 Remote sensing

In the current study, the Advanced Spaceborne Thermal

Table 1 Characteristics of ASTER and Sentinel 2 data

	ASTER			Sentinel 2	
Band	Central wavelength (μm)	Spatial resolution (m)	Band	Central wavelength (μm)	Spatial resolution (m)
1	0.560	15	1	0.443	60
2	0.660	15	2	0.490	10
3N	0.820	15	3	0.560	10
3B	0.820	15	4	0.665	10
4	1.650	30	5	0.704	20
5	2.165	30	6	0.740	20
6	2.205	30	7	0.782	20
7	2.260	30	8	0.842	10
8	2.330	30	8a	0.865	20
9	2.395	30	9	0.945	60
			10	1.375	60
			11	1.610	20
			12	2.190	20

Emission and Reflection Radiometer (ASTER) and Sentinel 2 (S2) data were integrated to discriminate the exposed lithologies and delineate the hydrothermal alterations in zones of prospective mineralization. The former was picked out due to its prominent applications in geological explorations, while the latter was mainly selected due to its higher spatial resolution that may help detailed investigations (Yu et al., 2012; Pour and Hashim, 2014; Othman and Gloaguen, 2017; Manap and San, 2018; Shebl et al., 2021).

ASTER is mounted on the Terra satellite platform to collect data in the visible and near-infrared, shortwave infrared, and thermal infrared regions (Table 1; Shebl et al., 2022). A digital mosaic created from four cloud-free level 1T Aster images was utilized to differentiate lithologies and identify the research area's distinctive structural features and favorable mineral alterations.

Sentinel 2 (developed by the European Space Agency (ESA) and launched in 2015) provides an updated level of earth observation through a 5-day revisit period, 13 spectral bands, and higher spatial resolution (up to 10 m), as shown in Table 1. All these characteristics are appropriate for detailed geological studies. Over the last decade, Sentinel 2 data has been used to map lithological and hydrothermal alteration (Van der Meer et al., 2014; Javhar et al., 2019; Shebl and Csámer, 2021; Kumar et al., 2022; Serbouti et al., 2022). In the current investigation, a cloud free scene was acquired through Copernicus Open Access Hub, radiometrically corrected, georeferenced (World Geodetic System 1984 (WGS 84) zone 36) and handled utilizing Sentinel Application Platform (SNAP) and QGIS software. For the detailed recognition of gold-controlling structural zones and shear sense indicators, a high resolution (2.5 m) Panchromatic Remote-sensing Instrument for Stereo Mapping (PRISM) dataset was implemented in the current study. PRISM was carried out on the Japanese Advanced Land Observing Satellite (ALOS) to provide high-resolution digital elevation models (DEMs).

Toward deciphering the lithological and hydrothermal alteration patterns, various efficient techniques including false color combination (FCC) (Abd El-Wahed et al., 2019; Hamimi et al., 2020), band ratio (BR) (Abdeen et al., 2001; Gad and Kusky, 2006; Van der Meer et al., 2014; El-Magd et al., 2015) and directed principal component analysis (Pour et al., 2018; Testa et al., 2018; Shebl et al., 2021) were applied. Principal component analysis (PCA) is a well-known image processing technique for decreasing the correlation among the utilized bands that could allow better discrimination of lithological and hydrothermal alteration features compared to the original bands. Specifying certain inputs for this analysis may highlight particular features or types of alterations depending mainly on the spectral characteristics of the utilized input bands or their transformations. Hence, the name DPCA is considered a type of PCA that is applied only to some bands or band ratio transformations to directly detect some desired features (Fraser and Green, 1987; Carranza and Hale, 2022; Shebl et al., 2021).

Additionally, the Maximum Likelihood classifier (MLC) is applied to outline mineralized zones over the whole investigated area, based on the hydrothermal alteration patterns deduced from the ASTER BR image. MLC is considered one of the most commonly used parametric classifiers for lithological allocation, which mainly depends on the statistical probability distributions of the generated classified classes. MLC has introduced a reasonable lithological generalization utilizing several datasets, including Advanced Land Imager (Shebl et al., 2022), Sentinel 2, ASTER, Landsat OLI, and Sentinel 1 data (Yu et al., 2012; Shebl and Csámer, 2021). The linear traces of structural features (faults and dikes) were extracted automatically through the application of directional filter (DF) details. The directional filter, also known as the directional sun angle filter, is a type of high-pass spatial filter that was used to enhance interpreting linear features of geological interest (Mavrantza and Argialas, 2003). The DF are directional edge enhancement filters that highlight edges perpendicular to a specific sun angle direction, namely to four fundamental directions (N–S, E–W, NE–SW, NW–SE). In this study, we used the N–S DF, which provides the highest level of linear feature enhancement and differentiation.

3.2 Aeromagnetic survey

The utilized total magnetic field (TMF) map of the study area (Fig. 7a) was implicated in the extensive airborne magnetic survey carried out by the Aero Service Division of Western Geophysical Company (1984) in Egypt as a part of ground water, hydrocarbon, and mineral assessment program. The survey was conducted using a Varian (V-85) proton precession magnetometer with special flight specifications (120 m of flight altitude in the NE direction, 1.5 km of traverse flight line spacing, and 10 km of tie line spacing).

The reduced to pole (RTP) map is a necessary step for positioning magnetic anomalies above their causal sources and alleviating issues associated with the total magnetic field map, which exhibits a complex structure for the detected magnetic anomalies. Therefore, the following enhancement techniques to be used in our study are derived from the reduced to pole map (Fig. 7b) of the total magnetic grid.

(1) Total gradient (TG). The method is also termed analytic signal (AS) and is defined as the square root of

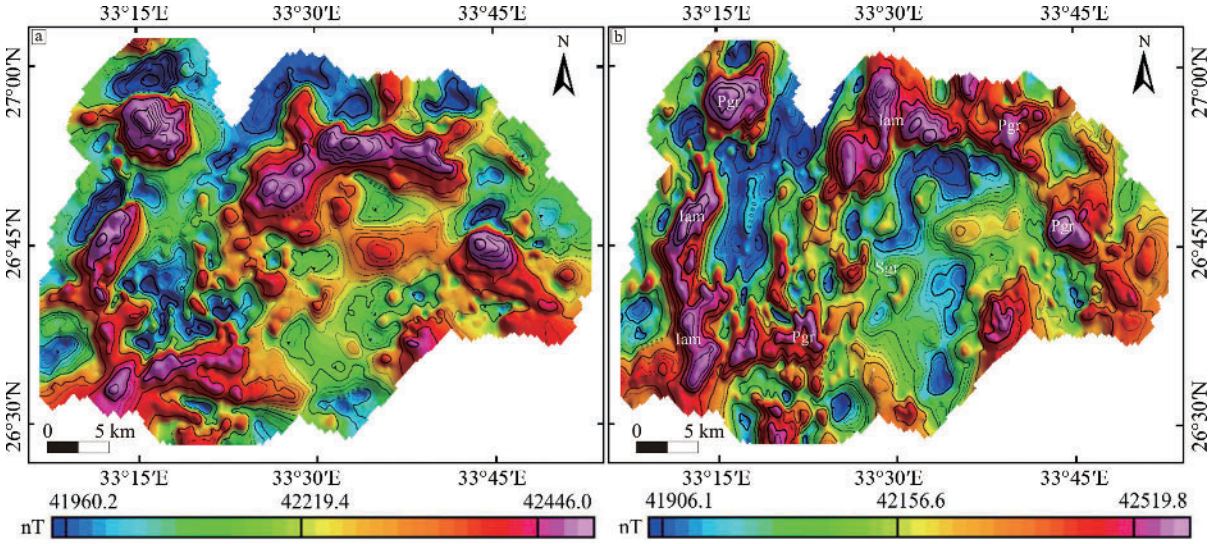

Fig. 7. Aeromagnetic data of the Fatira–Abu Zawal area showing: (a) total magnetic intensity map; (b) reduced to pole map.

the sum of the squares of the vertical (z) and the two-horizontal derivatives (x and y) of the total magnetic field (Nabighian, 1972, 1974). It is vertically independent of the magnetic inclination and better than RTP at interpreting magnetic anomalies in the middle and low altitudes. It precisely detects the edges of causative sources.

(2) Tilt derivative (TD). The filter is defined by Miller and Singh (1994), as TD = $\tan^{-1}(VD/THD)$, where *VD* and *THD* are the first vertical and horizontal derivatives of the total magnetic field, respectively. It is highly suitable for mapping shallow basement structures.

(3) 3D Euler deconvolution. The method encompasses the orthogonal gradients of the potential field in the *X*, *Y*, and *Z* directions and its usual equation (Thompson, 1982; Reid et al., 1990) is given as:

$$(x-x_0)\frac{\partial t}{\partial x}+(y-y_0)\frac{\partial t}{\partial y}+(z-z_0)\frac{\partial t}{\partial z}=N(B-T)$$

where T is the measured field at (x, y, z) and x_0, y_0, z_0 are coordinates, N is the structural index, and B is the field base level. This method determines the depth of different magnetic sources.

(4) Centre for exploration targeting (CET) grid analysis. It represents a recent technique that proposes a suite of algorithms to automatically delineate lineaments as a reliable indication of geological structures, combining textural analysis and contrast invariable ridge detection to locate laterally continuous textural ridges. The resultant lineaments are used to construct structural complexity heat maps (e.g., feature orientation entropy) for localizing favorable areas of ore deposits (Holden et al., 2008; Core et al., 2009). The mineralized areas relate to the structurally complex regions which are produced from the intersection of linear features (faults, dykes, ridges, etc.), serving as channels for hydrothermal solutions. These features are considered the criteria for the probability of occurrence of mineralization. In our study, a suite of maps, including standard deviation, phase symmetry, and

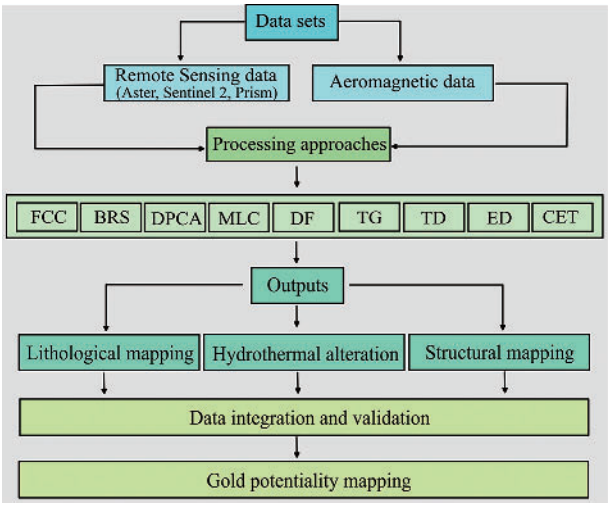

Fig. 8. Flowchart approach utilized in the current study.

vectorization maps, are used to generate the entropy heat map as a final map for characterizing the mineralization zones. A detailed workflow provides a summary of the integrated datasets' workflow and processing techniques (Fig. 8).

4 Results

4.1 Remote sensing results

Reasonable lithological discrimination (particularly granitic and mafic intrusive bodies) and structural demarcation are achieved through ASTER FCC (B7/B3/B1 in RGB) as shown in Fig. 9. This band combination enables to distinguish the curved boundary contacts of Barud syn-orogenic granodiorite, notably different from the straight normal fault contact in the SW to Abu Zawal sheared metavolcanics. The semicircular zonation of the post-orogenic granitoids on the SE side of the FSZ (i.e., near Gebel Ras Barud) indicates successive magmatism

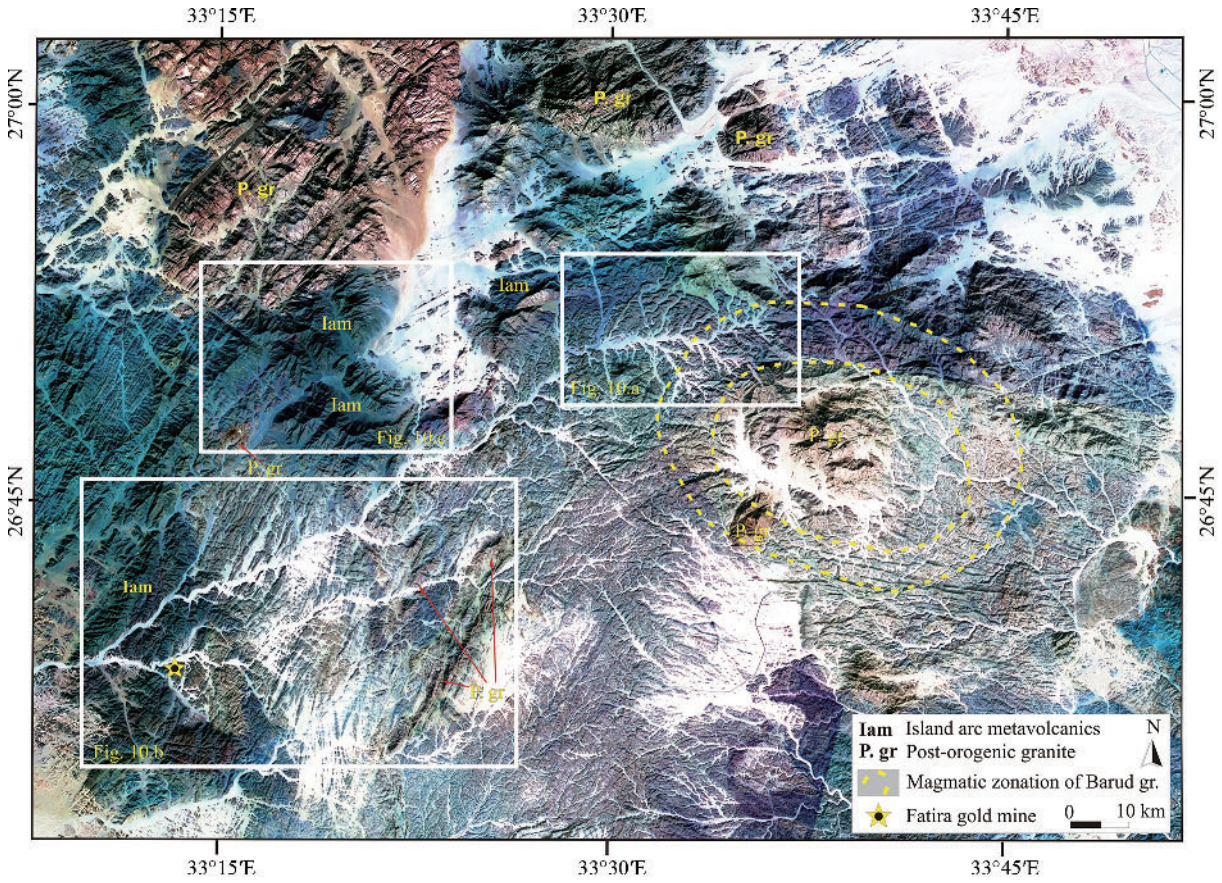

Fig. 9. Aster false color composite image (RGB:7/3/1) of the Fatira–Abu Zawal area.

accompanied by late-stage crustal differentiation. Moreover, numerous structural offset patterns are developed, which are exclusively related either to the island arc metavolcanics (dark blue areas) or to post-orogenic granites (brown hues) and dikes, indicating multiple stages of deformation (Fig. 9).

The pervasive macroscale z-fold pattern of Fatira metavolcanic (Figs. 9, 10a, b) and its parasitic folds, as well as the large-scale sigma-like fabric of blocks and dikes of the Abu Zawal granites, outline the FSZ's southern boundary (Figs. 9, 10c). The FSZ extends for about 40 km in length and 15–20 km in width eastward, roughly in a NE to ENE direction. North of Barud granodiorites, the Fatira metavolcanic belt is shifted laterally on the FSZ northern boundary for about 2.5 km (Figs. 9, 10d). The Abu Zawal metavolcanics display offsets of discordant blocks through brittle subsets (Figs. 9, 10c).

To investigate the mineralization-related alterations, spectrally informative band ratios (BR) and directed principal component analyses (DPCA) are applied. Applying the band ratio combination of ASTER (RGB: B4/B2, B4/B5, B5/B6) was widely used to discriminate gossans from the host rock, which accomplished by classifying minerals into two groups: iron minerals and minerals found in hydrothermally altered rocks, such as calcite, clay, and chlorite-rich zones (Abdelsalam and Stern, 1999; Abdelsalam et al., 2000; Volesky et al., 2003). Red areas in the image (Fig. 11, Supp. Fig. 1) represent gossan (iron-rich) rocks, which are relatively scattered and localized. Green colors indicate hydrated alteration minerals, while yellow-colored areas are associated with both of the previous groups, representing areas of alteration potentially related to ore mineralization compared with the purple-hued color for quartz- and feldspar-dominated host rocks. These yellow regions are present sporadically in the Fatira and Abu Zawal areas, not only around the Fatira gold mine but also in the areas a, b, and c, which are associated with the emplacement of the sheared post-orogenic granites and sheeted felsite dikes (Figs. 3, 11).

The general hydrothermal alteration pattern is resolved through applying the ratios suggested by Sabins (1999) to Sentinel 2 data (B11/B12, B4/B2, B4/B11) as shown in Fig. 12a. A specific investigation of several types of hydrothermal alterations (mostly associated with the mineralized zones) was executed through BR and DPCA techniques, depending mainly on the spectral characteristics of the utilized bands. Consequently, the current study applied BRs for determination of hydroxyl-bearing minerals (B11/B12), Gossan (B11/B4), and DPCAs for iron oxides (through DPCA of bands B2, B4, B8a, B11) as shown in Fig. 12b, c, and d. After comparing these outputs and based on the estimated predictions from the band ratio (RGB: B4/B2, B4/B5, B5/B6; Fig. 11), potential mineralization and hydrothermal alteration

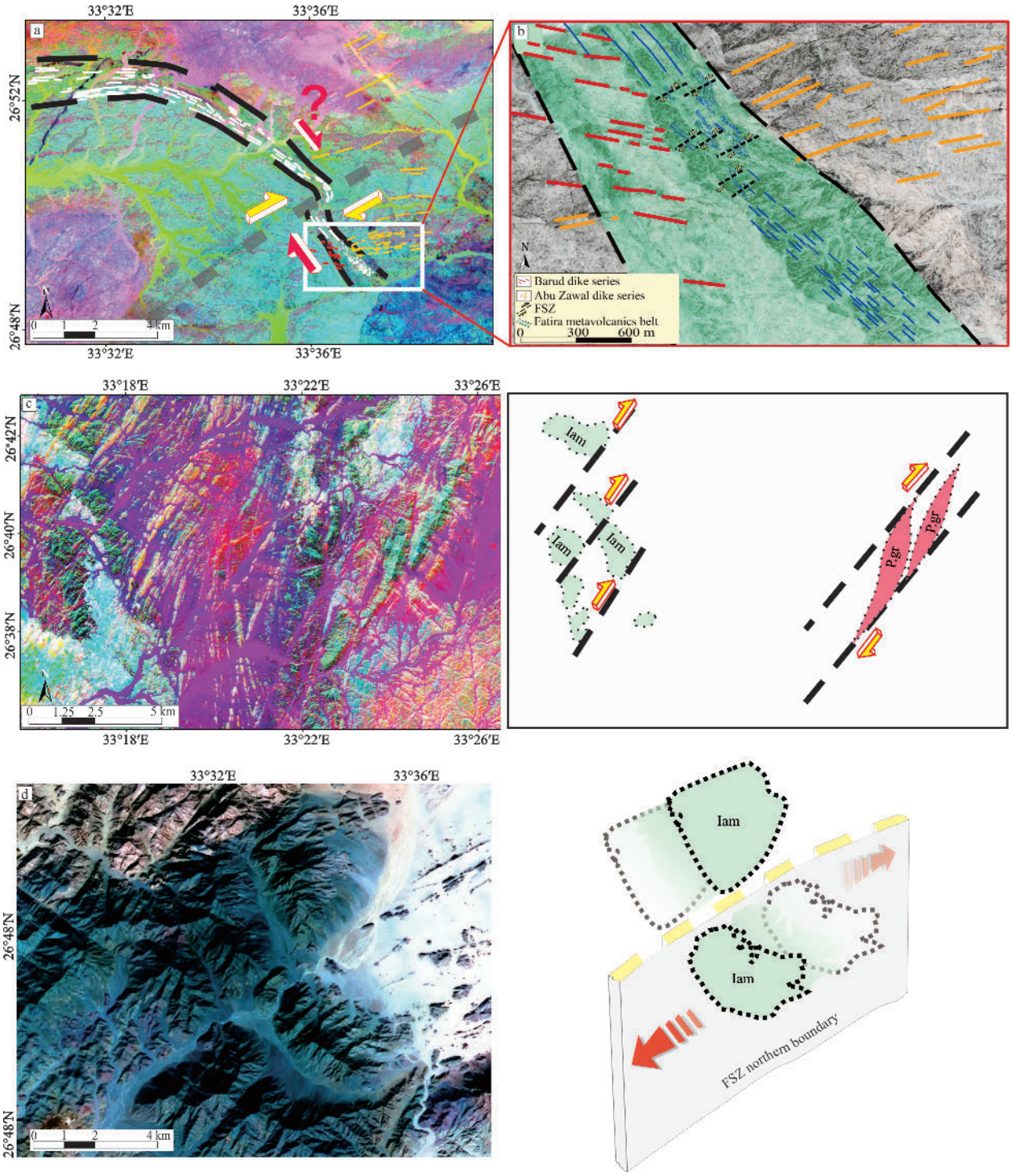

Fig. 10. (a) PCA (RGB b2, b4, b5) highlighting shear transformation over the northern part of FSZ; (b) sketch created from Google Earth for the southern portion of the Fatira metavolcanic belt, exhibiting parasitic z-folds and dike series (image©2022 Maxar technologies); (c) RGB BR of 11/12, 4/2, and 4/11 demarcates the dextral sense of shearing along a NE–SW striking fault set in the SW part of the Barud granitoids and the Abu Zawal metavolcanics; (d) Aster FCC (RGB: 731) showing the dextral dislocation of Fatira metavolcanic belt, pan-sharpened (using PRISM).

locations (i.e., yellow zones) are categorized using Maximum Likelihood Classification (MLC) (Fig. 13).

Together with the spatial distribution of the hydrothermal alterations, the structural lineaments are extensively important to delineate the potential zones. Consequently, the DF is applied to discern and interpret some of the

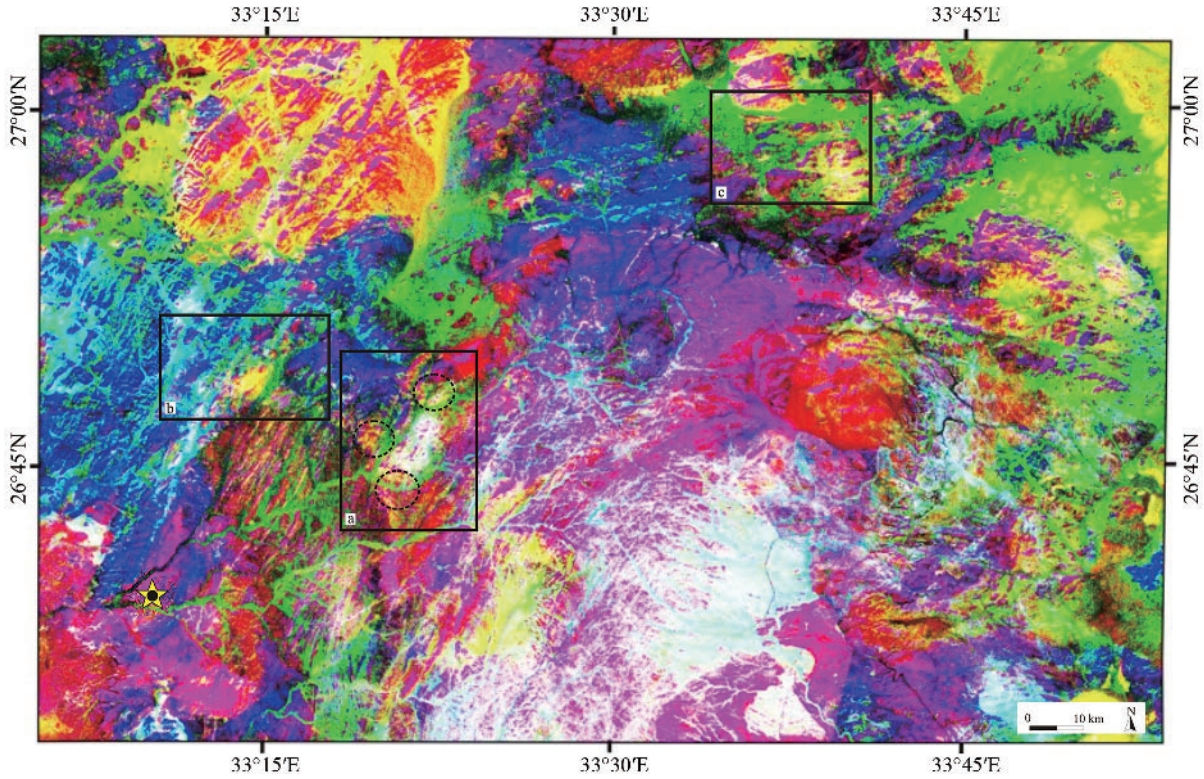

Fig. 11. ASTER BR (RGB: B4/B2, B4/B5, B5/B6), highlighting gossan (red), alteration minerals (green to yellow), especially at regions a, b, and c, and host rock (blue to purple).

structural lineaments' relationships. The result of N–S DF, as shown in Fig. 14a and Supp. Fig. 2, is potentially the best method to enhance and elucidate the southern boundary of the FSZ, along which the Fatira metavolcanic z-fold has been dislocated. Moreover, the two phases of the dikes of the Abu Zawal and Barud areas are perfectly discriminated based on their directions, which extend roughly to NE–SW and NW–SE, respectively. These trends are roughly conformable with the direction of the main wadis, particularly Wadi Fatira, Abu Zawal, and Wadi Barud (Figs. 3, 14b, c).

4.2 Aeromagnetic results

The visual inspection of the AS map reveals the most predominant features, which are characterized by the high analytical signal amplitude aligning roughly to NE FSZ, NW, and NS directions along the northern and northwestern parts of the area (Fig. 15a, b). Three magnetic zones are well defined on the map and correlated with their lithological composition based on the overlapping of the geological map (Fig. 3). The high magnetic anomalies are related to island arc metavolcanics, intrusive gabbros, and granites. The medium and low magnetic anomalies are associated with granodiorite and gneissic rocks. According to Salem et al. (2007), the TD (Fig. 15b) derived from the RTP grid can be used to delineate structural features (e.g., faults, contacts, and the edges of magnetic sources). The zero contour lines (yellow color) indicate vertical and horizontal edges of concealed magnetic structures (e.g., contact location and direction). The main interpreted structural trends from the TD map are NE, NS, NW, and NNE, which show a good match with the sketched faults in Fig. 8a, b.

Applying the Standard Euler Deconvolution approach to the RTP grid map using structural indexes of 0 and 1 was perfect to define contact and fault models, respectively. Assuming a contact model with a moving window of 9 × 9 data points, the first scenario is used to detect probable subsurface structures with a 5% relative inaccuracy. The source location is represented by symbols exhibiting the estimated depth values, which range from 0 to a bit little more than 3000 m (Fig. 15c), and most depths fall between 0 and 1000 m, indicating shallow magnetic sources. Also, the Euler solutions indicated that the main trends of contacts are NE, NNE, and NW. The second scenario assumes a fault model (Fig. 15d) showing estimated depths ranging from 0 to more than 3000 m, and the majority of them are from 1000 m to 2500 m, indicating deep sources. In this case, the main trends in this case are the same as those identified in the contact model.

The CET grid analysis in such a study was applied to the aeromagnetic data in the form of an RTP grid for locating high potential areas of mineralization occurrences by generating a series of structural complexity maps. Starting with the standard deviation (STD), which features the discontinuity zones of the area (Fig. 16a). Then the STD is used to compute the phase symmetry map (Fig. 16b), defining the probable areas of interest. The map reveals a primary indication of the automated lineaments to be generated after applying a set of processing steps that

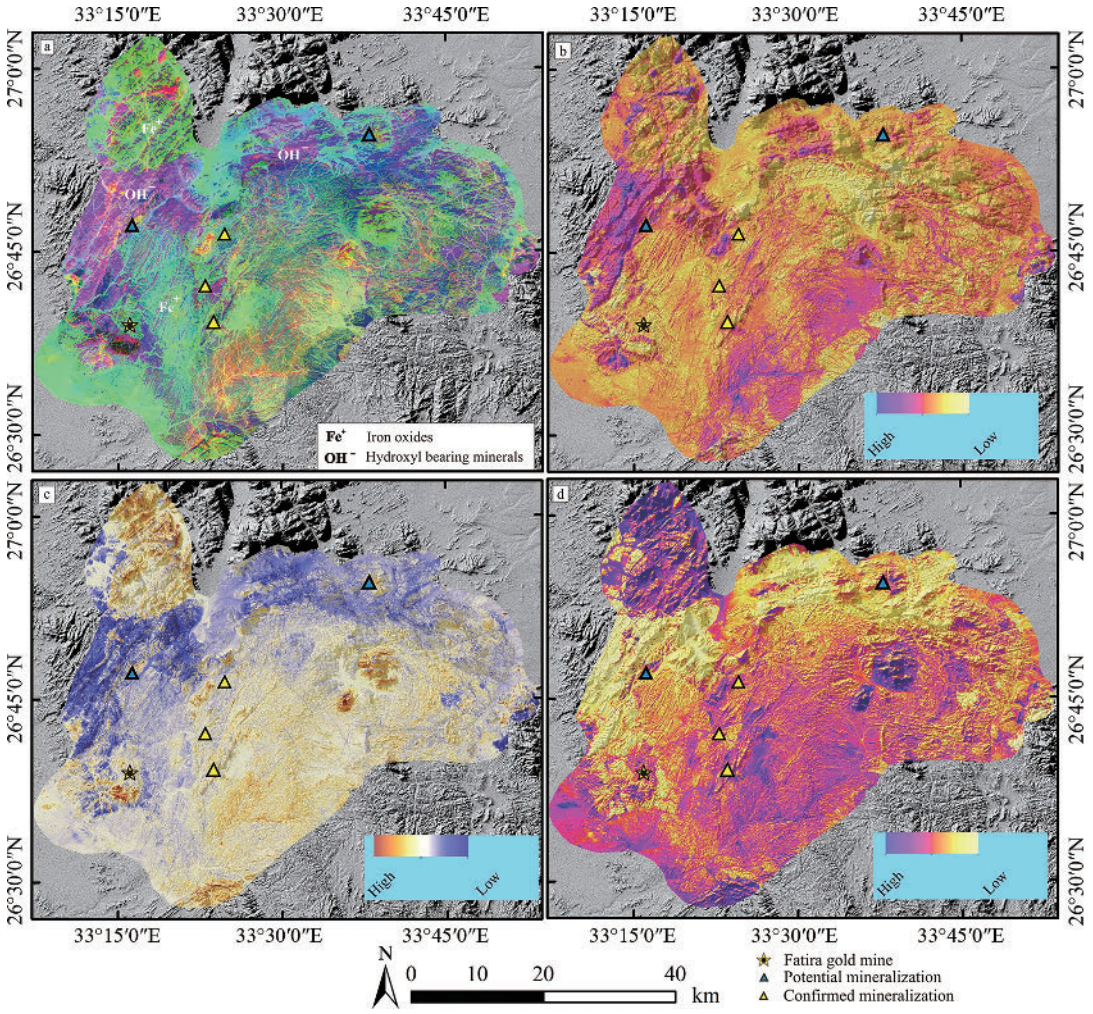

Fig. 12. Maps of indices calculated for mapping of various features: (a) Sabins ratio depicting the general hydrothermal alteration pattern; (b) hydroxyl-bearing minerals (11/12); (c) gossan (11/4); (d) iron oxides (through DPCA of bands 2, 4, 8a, 11).

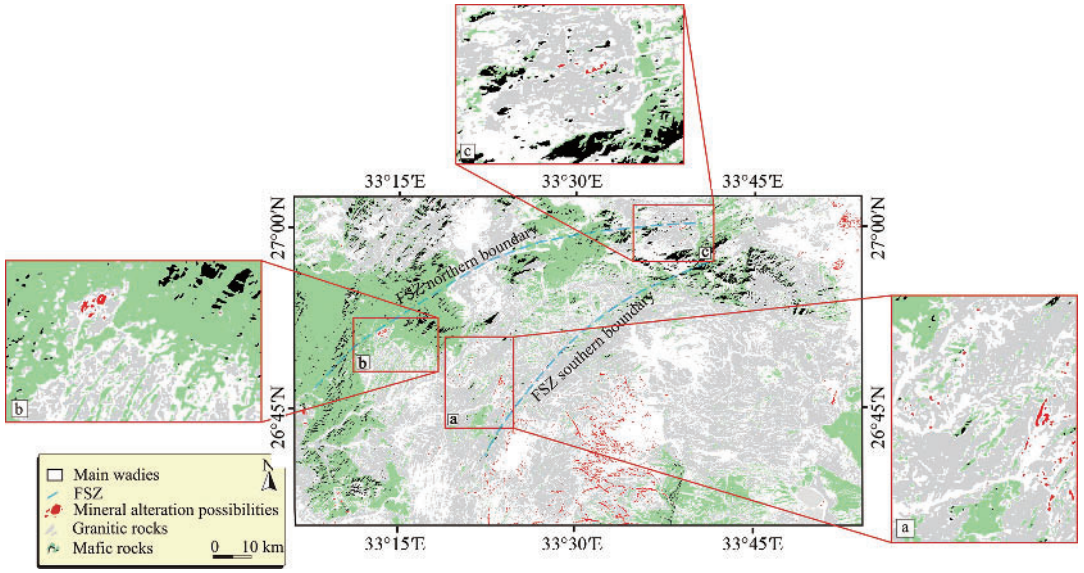

Fig. 13. Supervised classification image (MLC) of Fatira–Abu Zawal area showing the mineral alteration possibilities relative to the FSZ.

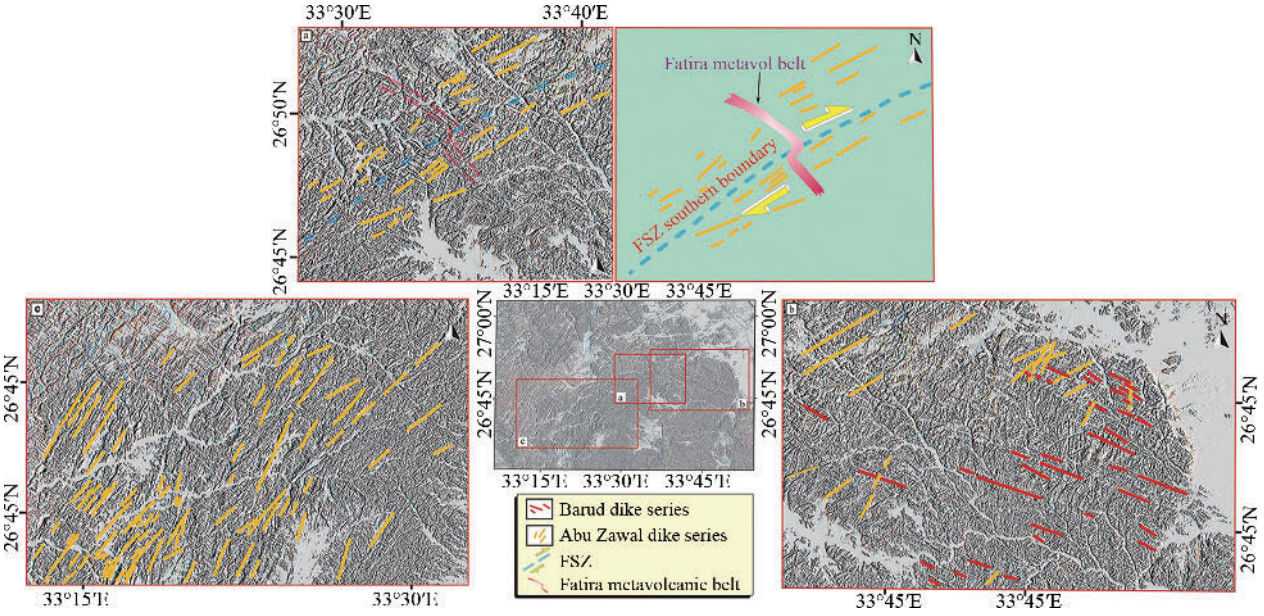

Fig. 14. N–S directional filter and extracted lineaments of Fatira–Abu Zawal area showing: (a) the dislocation of Fatira metavolcanic belt along the southern boundary of FSZ, aligned with Abu Zawal dikes; (b) the NE–SW Abu Zawal dikes; (c) the NW–SE Barud dikes.

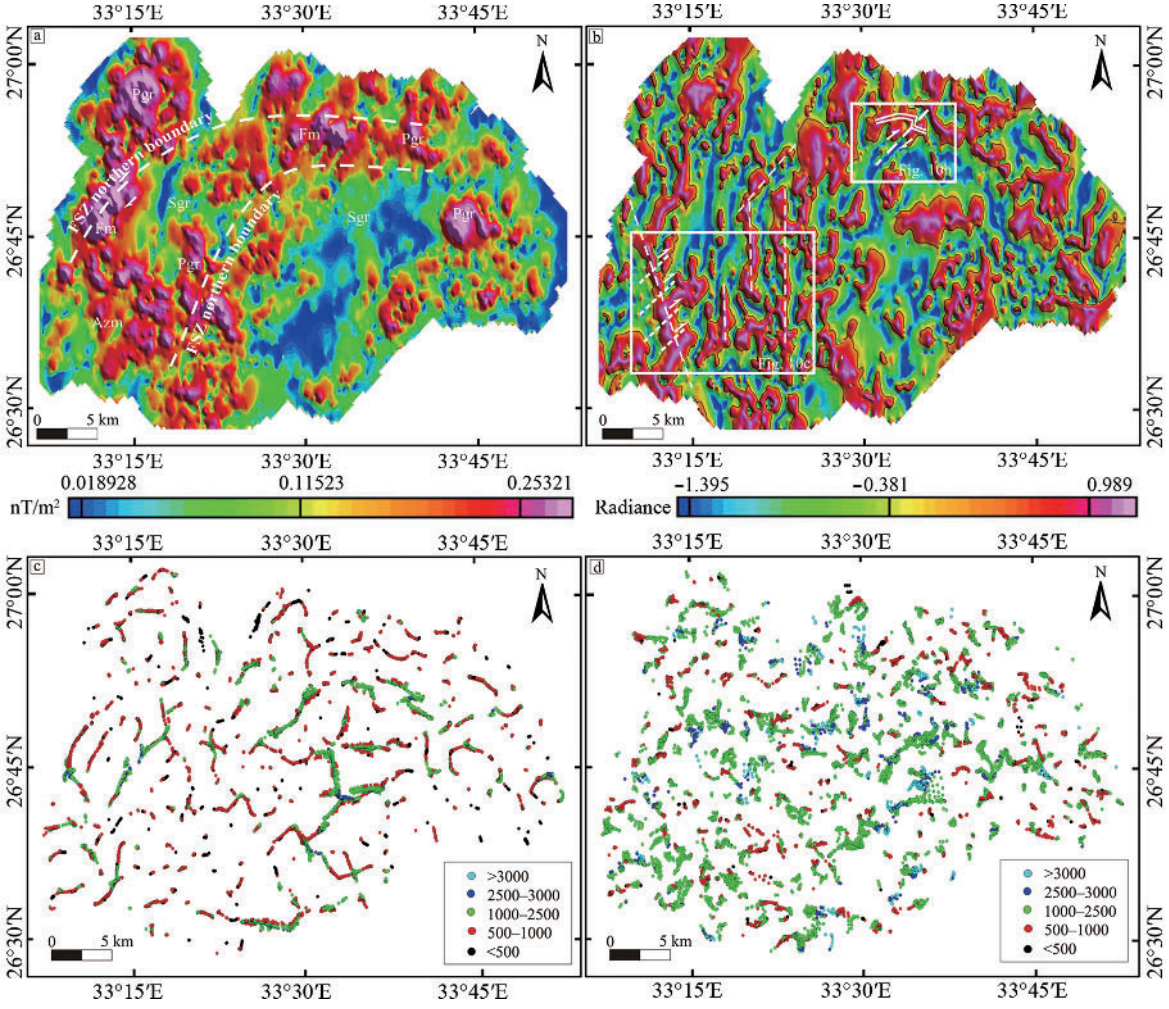

Fig. 15. (a) Analytical signal displaying major structural lineaments of Fatira–Abu Zawal area; (b) tilt derivative showing the key structural patterns of the study area; (c) standard Euler deconvolution with SI = 0; (d) standard Euler deconvolution with SI = 1.

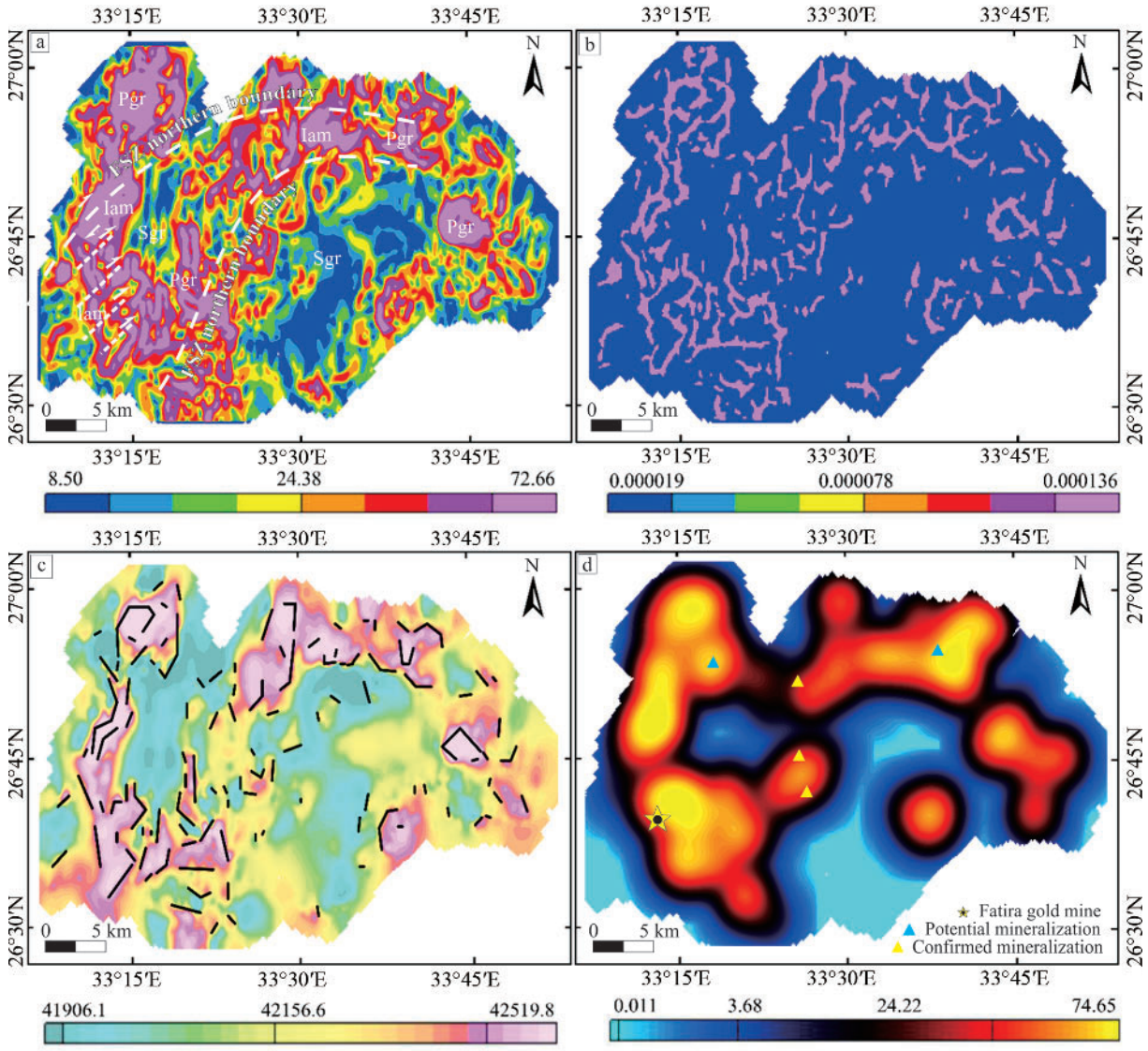

Fig. 16. CET outcomes: (a) standard deviation observing the main lithologies and FSZ structural features; (b) phase symmetry; (c) vectorized lineaments; (d) entropy heat map showing the probable mineralized sites.

involve thresholding, skeletonization, and vectorization. At first, thresholding which applies non-maximal suppression (NMS), is utilized to reduce the phase symmetry to a grid that only depicts the trend lines, while NMS is useful to find ridges since the low values are suppressed while points of local maxima are preserved. Then, skeletonisation reduces feature regions to thin lines, and skeleton to vectors exports the skeletal thin lines to vectors. To end up with the output of the latter step (vectorization) that exhibits the automated detected lineaments (Fig. 16c). It is worth noting that the main detected trends are oriented in the NE, NNE, and NW directions. After all, the orientation entropy heat map (Fig. 16d), which defines the favorable areas of ore deposits, is derived by using the vectorized lineaments. A glance at the entropy heat map reveals six regions that can be defined as beneficial for mineralization indicated by highest values (up to 74) which represent the strongest predicted mineralized zones. These areas, which are conformable with the three zones (a, b, and c; Figs. 11–13), derived from remote sensing data, beside the Fatira gold mine, are noted to be along the FSZ and related structural areas. In general, the structures and probable mineralized zones defined by the analysis of aeromagnetic maps agreed with those interpreted from remote sensing data.

5 Discussion

In this study, extensive PAO-related tectonic events have been observed in the Fatira region, evidenced by integrated multi-source data that exhibits the diversity of rock types in the research area. These tectonic events displayed various deformational features that resemble a typical gradual transition from a deep-seated ductile regime to brittle shearing at a shallow crustal level.

Among these features, the NE- to ENE-trending, highly sheared, almost vertical Fatira metavolcanic belt, which is aligned with the gneissic bands of the originally intrusive syn-orogenic Barud magmatic body, demonstrates multistage deformation. The z-shaped fold pattern of this belt, which is displaced dextrally along the southern boundary of the FSZ (Figs. 4c, 10a, b), is also accompanied by the coeval Abu Zawal dike sets in the NE–SW direction (Figs. 10a, 14a), suggesting that the FSZ has experienced an earlier ductile phase of deformation. These dikes developed with post-orogenic granites along a transtensional shear array, which culminates the evolutionary system associated with the PAO's tectonic escape to the north. These deformational features are investigated in nine field observations that observe dextral shear sense of movement along FSZ, including rotated-type core-mantle fabrics, S-C fabrics, extensional gashes, and boudinage structures, which require more detailed description (Makroum et al., in prep.). So, the FSZ can be thought to have started with ductile deformations, possibly at a deeper crustal level, extending roughly in the ENE–WSW direction with dextral motions that seem to have continued to experience later brittle deformations (Fig. 17).

It is likely that such a tectonic environment, particularly the cessation of the ANS arc-terrane, which witnessed the evolution of post-orogenic granites and felsite dikes, will serve mostly as a competent structural host for ore deposition (e.g., gold deposits). In the heavily sheared post-orogenic granite bodies, NE–SW striking extensional shear fractures were observed in outcrops that would be potential channels for hydrothermal fluid transfer. The studied petrographic thin sections of these granites, especially the highly sheared ones, show a high abundance of alteration minerals, such as iron oxides, chlorite, calcite, and kaolinite, indicating propylitic alteration, which is commonly associated with ore deposits (Fig. 6d, e). Furthermore, the integrated remote sensing and geophysical datasets detected and confirmed the wide development of this hydrothermal alteration mineral assemblage associated with ore deposits. The detailed mapping of the region with the supervised classification of the selected mineralized sites reveals that the mineral alterations associated with the ore deposits are aligned with the NE–SW oval-shaped post-orogenic granites and felsite dikes of the Abu Zawal area. The structures controlling these alterations developed in a transtensional phase of FSZ.

Moreover, the occurrence potential of these alterations would be increasingly present along the FSZ contact boundary between lithologies of different protolith: between Abu Zawal post-orogenic granites and gabbros or Fatira metavolcanics (i.e., zones a, b, and c, respectively). This perspective sheds light on the structural control of the FSZ on the localization of ore deposits.

The application of the integrated approaches to locate

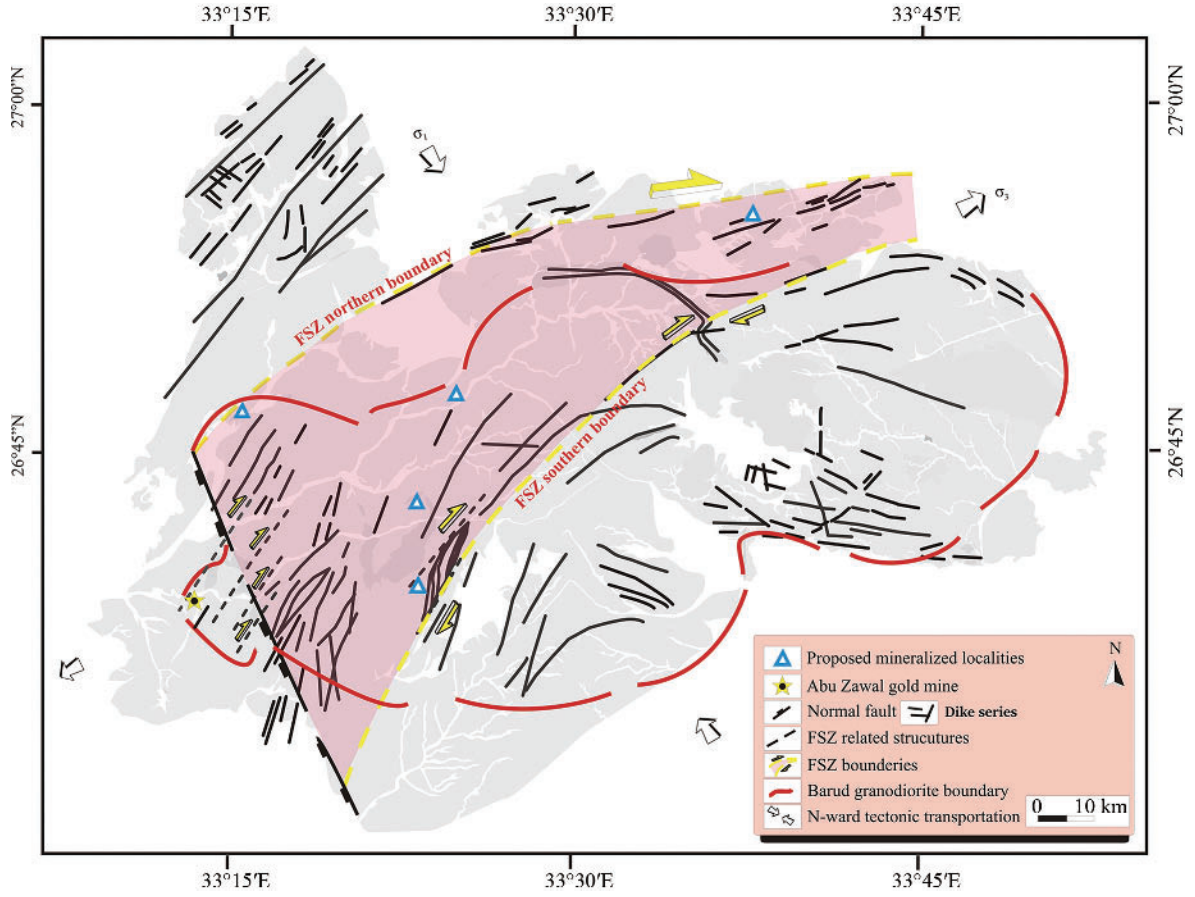

Fig. 17. Tectonic model for the deformational events of the Fatira–Abu Zawal area, Eastern Desert, Egypt.

the three proposed mineral alteration zones is highly trusted, as demonstrated by zone a, which exhibits a high degree of match to the metal deposits documented at the Fatira gold mine, Gebel El Urf, Gebel Abu Kharif, and Gebel El Dob (Abu El-Leil et al., 2015; Draz et al., 2017; Abd El Monsef et al., 2020).

6 Conclusions

Spatial overlay analysis of remote sensing and aeromagnetic maps, in conjunction with field observations, revealed the ability of the remotely integrated techniques to achieve an acceptable degree of reliability and efficiency in localizing structurally-controlled mineral alterations compared with the traditional fieldwork. In this regard, the present research has yielded the following results:

(1) Several potential mineral alteration localities are linked to gold mineralization within the studied area (zones a, b and c). They are completely controlled by FSZ and mostly hosted by sheared post-orogenic granitic rocks and felsite dikes. These probable localities have been confirmed and are supposed to be promising with appropriate regime that is highly altered, structurally dissected, and characterized by highly magnetic anomalies.

(2) The study accentuated the critical role of geological key structures in controlling gold mineralization, and supported further investigations not only in Fatira area, but also over the whole northern part of the Egyptian Eastern Desert using a newly proposed tectonic model.

(3) The constructed tectonic model may pave the way for extensive examinations of sheared post-orogenic granitic rocks displaying indications of shear deformation. Considering this, the tectonic environment that displays a transition from transpression to a transtension phase may offer the structural network that allows and eases the migration of metamorphic and hydrothermal fluids to low-pressure regions, which are highly recommended sites for gold concentration.

In conclusion, further ore analysis can be conducted to estimate the extraction potential of the identified zones.

Acknowledgments

The Egyptian ministry for higher education and the Stipendium Hungaricum scholarship are thanked for funding the first and third authors under the joint executive program between Hungary and Egypt.

Manuscript received Feb. 11, 2022
accepted Oct. 18, 2022
associate EIC: CHI Guoxiang
edited by FANG Xiang

Supplementary data to this article can be found online at https://doi.org/10.1111/1755-6724.15019.

Reference

Abd El Monsef, M., Slobodník, M., and Salem, I.A., 2020. Characteristics and nature of gold-bearing fluids in Fatira area, North Eastern Desert of Egypt: Possible transition from intrusion-related to orogenic deposits. Arabian Journal of Geosciences, 13: 1034.

Abd El Monsef, M., Slobodník, M., and Salem, I.A., 2018. Hydrothermal evolution of granitoid-hosted gold mineralization in gidami area: An example for orogenic-gold deposits in Egypt. Journal of African Earth Sciences, 146: 132–149.

Abd El-Nabi, H.H., 1977. Result of prospecting for mineral resources of Wadi Hammad, El-Atshan, El-Ghoza and Fatira El-Beida area. Cairo: Internal report EGSMA, Technoexpert, Cairo.

Abd El-Wahed, M., Kamh, S., Ashmawy, M., and Shebl, A., 2019. Transpressive structures in the Ghadir shear belt, Eastern Desert, Egypt: Evidence for partitioning of oblique convergence in the Arabian–Nubian Shield during Gondwana Agglutination. Acta Geologica Sinica (English Edition), 93: 1614–1646.

Abdeen, M.M., Thurmond, A.K., Abdelsalam, M.G., and Stern, R.J., 2001. Application of ASTER band-ratio images for geological mapping in arid regions: The neoproterozoic Allaqi Suture, Egypt. In: Proceedings of GSA 2001 Annual Meeting, Boston.

Abdelkareem, M., El-Din, G.M.K., and Osman, I., 2018. An integrated approach for mapping mineral resources in the Eastern Desert of Egypt. International Journal of Applied Earth Observation and Geoinformation, 73: 682–696.

Abdelsalam, M., and Stern, R., 1999. Mineral exploration with satellite remote sensing imagery: Examples from the Neoproterozoic Arabian–Nubian Shield. Journal of African Earth Sciences, 28(4): 1.

Abdelsalam, M.G., Stern, R., and Berhane, W.G., 2000. Mapping gossans in arid regions with Landsat TM and SIR-C images: The Beddaho alteration zone in northern Eritrea. Journal of African Earth Sciences, 30: 903–916.

Abu El-Leil, I., Tolba, S.I., and Shahin, T.M., 2015. Mineralogical studies of placer Wadi deposits of Gabal El-Dob area, North Eastern Desert, Egypt: A good preliminary tool for prospecting ores in Arabian–Nubian Shield. International Journal of Innovative Science Engineering and Technology, 2(10): 68–93.

Abu-Alam, T., Abd El Monsef, M., and Grosch, E., 2019. Shear-zone hosted gold mineralization of the Arabian–Nubian Shield: Devolatilization processes across the greenschist–amphibolite-facies transition. Geological Society, London, Special Publications, 478(1): 287–313.

Abu-Alam, T., Abd El Monsef, M., and Grosch, E., 2018. Shear-zone hosted gold mineralization of the Arabian–Nubian shield: Devolatization processes across the greenschist–amphibolite facies transition. In: Ferrero, S., Lanari, P., Goncalves, P., and Grosch, E.G. (eds.), Metamorphic Geology: Microscale to Mountain Belts. Geological Society, London, Special Publications, 478. DOI: 10.1144/SP478.13.

Aero Service Division of Western Geophysical Company. 1984. Final operational report of airborne magnetic/radiation survey in the Eastern Desert, Egypt. Geological Report: For the Egyptian General Petroleum Corporation (EGPC) and the Egyptian Geological Survey and Mining Authority (EGSMA).

Akaad, M.K., El-Gaby, S., and Habib, M.E., 1973. The Barud Gneisses and the origin of Grey Granite. Bulletin of the Faculty of Science, 2: 55–69.

Azzaz, S.A., Sabet, A.H., Soliman, M.M., and Botros, N.S., 1997. Mode of occurrence and genesis of the gold mineralizations in the North Eastern Desert of Egypt. Egypt, Mineral, 9: 169–185.

Botros, N.S., 1991. Geological and geochemical studies on some gold occurrences in the North Eastern Desert, Egypt (Ph.D. thesis). Zagazig University, 1–146.

Botros, N.S., 2004. A new classification of the gold deposits of Egypt. Ore Geology Reviews, 25(1–2): 1–37.

Carranza, E.J.M, and Hale, M., 2002. Mineral imaging with Landsat Thematic Mapper data for hydrothermal alteration mapping in heavily vegetated terrane. International Journal of Remote Sensing, 23(22): 4827–4852.

Core, D., Buckingham, A., and Belfield, S., 2009. Detailed structural analysis of magnetic data—Done quickly and

objectively. SGEG Newsletter, 1(2): 15–21.
Draz, O.M., El-Alfi, S.M., and Esmail, E.M., 2017. Mineralogical and radiometrical studies of Gabal El-Dob area, Central Eastern Desert, Egypt. Current Science International, 6(1): 103–120.
El Gaby, S., List, F.K., and Tehrani, R., 1988. Geology, evolution and metallogenesis of the Pan–African belt in Egypt. In: El Gaby, S., and Greiling, R. (eds.), The Pan-African belt of NE Africa and adjacent areas, Tectonic evolution, and economic aspects. Freidr. Vieweg&Sohn, Braunschweig/Weisbaden, 17–68.
Eldosouky, A.M., Abdelkareem, M., and Elkhateeb, S.O., 2017. Integration of remote sensing and aeromagnetic data for mapping structural features and hydrothermal alteration zones in Wadi Allaqi area, Southeastern Desert of Egypt. Journal of African Earth Sciences, 130: 28–37.
El-Magd, I.A., Mohy, H., and Basta, F., 2015. Application of remote sensing for gold exploration in the Fawakhir area, Central Eastern Desert of Egypt. Arabian Journal of Geosciences, 8: 3523–3536.
Fraser, S.J., and Green, A.A., 1987. A software defoliant for geological analysis of band ratios. International Journal of Remote Sensing, 8(3): 525–532.
Fritz H., Wallbrecher, E., Khudeir, A.A., Abu El Ela, F., and Dallmeyer, R.D., 1996. Formation of Neoproterozoic metamorphic core complexes during oblique convergence (Eastern Desert, Egypt). Journal of African Earth Sciences, 23: 311–329.
Gad, S., and Kusky, T., 2006. Lithological mapping in the Eastern Desert of Egypt, the Barramiya area, using Landsat thematic mapper ™. Journal of African Earth Sciences, 44: 196–202.
Ghazala, H., Aboelkhair, H., and Thabet, W., 2021. Integration of ASTER and geophysical data for delineating potential mineralization zones in Dungash–Atud area, Central Eastern Desert, Egypt. Arabian Journal of Geosciences, 14(6): 1–22.
Greiling, R.O., Kröner, A., El-Ramly, M.F., and Rashwan, A.A., 1988. Structural relationship between the southern and central parts of the Eastern desert of Egypt: Details of a fold and thrust belt. In: El-Gaby, S., and Greiling, R.O. (eds.), The Pan-African Belt of Northeast Africa and Ddjacent Areas. Weisbaden: Vieweg & Sohn, 121–146.
Hamimi, Z., Hagag, W., Kamh, S., and El-Araby, A., 2020. Application of remote-sensing techniques in geological and structural mapping of Atalla Shear Zone and Environs, Central Eastern Desert, Egypt. Arabian Journal of Geosciences, 13: 414.
Haroun, R.G., 2001. Metallogenic studies on Wadi Fatira area, Eastern Desert, Egypt (M.Sc. thesis). Ain Shams University, 1–289.
Harraz, H.Z., 2002. Fluid inclusions in the mesozonal gold deposit at Atud mine, Eastern Desert, Egypt. Journal of African Earth Sciences, 35: 347–363.
Hasan, E., Fagin, T., El Alfy, Z., and Hong, Y., 2014. Mapping of gold mineralization alteration zones in central Eastern Desert Egypt using spectral angular mapper and aeromagnetic data. In: AGU Fall Meeting Abstracts, NS43A-3879.
Helmy, H., Kaindl, R., Fritz, H., and Loizenbauer, J., 2004. The Sukari gold mine, Eastern Desert, Egypt: Structural setting, mineralogy and fluid inclusion study. Mineralium Deposita, 39: 495–511.
Holden, E.J., Dentith, M., and Kovesi, P., 2008. Towards the automated analysis of regional aeromagnetic data to identify regions prospective for gold deposits. Computers & Geosciences, 34: 1505–1513.
Hume, W.F., 1934. Geology of Egypt II, (1) The Metamorphic Rocks, and (2) The Later Plutonic and Minor Intrusive Rocks. Cairo: Government Press.
Hussein, A.A., 1990. Mineral deposits. In: Said, R., (ed.), The Geology of Egypt, Rotterdam: A.A. Balkema, 511–566.
Javhar, A., Chen, X., Bao, A., Jamshed, A., Yunus, M., Jovid, A., and Latipa, T., 2019. Comparison of multi-resolution optical Landsat-8, Sentinel-2 and radar Sentinel-1 data for automatic lineament extraction: A case study of Alichur area, SE Pamir. Remote Sensing, 11: 778.
Johnson, P.R., Andresen, A., Collins, A.S., Fowler, A.R., Fritz, H., Ghebreab, W., Kusky, T., and Stern, R.J., 2011. Late Cryogenian–Ediacaran history of the Arabian–Nubian Shield: A review of depositional, plutonic, structural, and tectonic events in the closing stages of the northern East African Orogen. Journal of African Earth Sciences, 61: 167–232.
Klemm, D.D., Klemm, R., and Murr, A., 2001. Gold of the Pharaohs–6000 years of gold mining in Egypt and Nubia. Journal of African Earth Sciences, 33(3–4): 643–659.
Klemm, R., and Klemm, D., 2013. Gold and gold mining in ancient Egypt and Nubia, Natural Science in Archaeology. Berlin, Heidelberg: Springer-Verlag, 341. DOI: 10.1007/978-3-642-22508-6_6
Kumar, C., Chatterjee, S., Oommen, T., Guha, A., and Mukherjee, A., 2022. Multi-sensor datasets based optimal integration of spectral, textural, and morphological characteristics of rocks for lithological classification using machine learning models. Geocarto International, 37(20): 6004–6032.
Kusky, T.M., Abdelsalam, M., Tucker, R., and Stern, R.J., 2003. Evolution of the East African and related Orogens, and the assembly of Gondwana. Special Issue, Precambrian Research, 123: 81–344.
Loizenbauer, J., Neumayr, P., and Fritz, H., 2002. Genesis of the Fawakhir gold deposit in the Eastern Desert of Egypt: The result of late Pan-African transpressional tectonics. 19th Colloquium of African Geology, El Jadida, Morocco, 120–121.
Manap, H.S., and San, B.T., 2018. Lithological mapping using different classification algorithms in western antalya, turkey. International Multidisciplinary Scientific GeoConference Surveying Geology and Mining Ecology Management (SGEM), 18: 551–556.
Mavrantza, O., and Argialas, D.P., 2003. Implementation and evaluation of spatial filtering and edge detection techniques for lineament mapping: Case study–Alevrada, Central Greece. In: Remote Sensing for Environmental Monitoring, GIS Applications, and Geology II, 4886: 417–428.
Miller, H.G., and Singh, V., 1994. Potential field tilt—A new concept for location of potential field sources. Journal of Applied Geophysics, 32(2–3): 213–217.
Moussa, E.M.M., Stern, R.J., Manton, W.I., and Ali, K.A., 2008. SHRIMP zircon dating and Sm/Nd isotopic investigations of Neoproterozoic granitoids, Eastern Desert, Egypt. Precambrian Research, 160: 341–356.
Murr, A., 1999. Die Genese der Goldlagerstättenbezirke Fatira, Gidami Atalla und Hangaliya in der Ägyptischen Ostwüste. Münchner Geologische Hefte, A27: 202.
Nabighian, M.N., 1972. The analytic signal of two-dimensional magnetic bodies with polygonal cross-section: Its properties and use for automated anomaly interpretation. Geophysics, 37 (3): 507–517.
Nabighian, M.N., 1974. Additional comments on the analytic signal of two-dimensional magnetic bodies with polygonal cross-section. Geophysics, 39(1): 85–92.
Othman, A.A., and Gloaguen, R., 2017. Integration of spectral, spatial and morphometric data into lithological mapping: A comparison of different Machine Learning Algorithms in the Kurdistan Region, NE Iraq. Journal of Asian Earth Sciences, 146: 90–102.
Pour, A.B., and Hashim, M., 2014. ASTER, ALI and Hyperion sensors data for lithological mapping and ore minerals exploration. SpringerPlus, 3: 130.
Pour, A.B., Park, T.Y.S., Park, Y., Hong, J.K., Zoheir, B., Pradhan, B., Ayoobi, I., and Hashim, M., 2018. Application of multi-sensor satellite data for exploration of Zn-Pb sulfide mineralization in the Franklinian Basin, North Greenland. Remote Sensing, 10: 1186.
Reid, A.B., Allsop, J.M., Granser, H., Millett, A.T., and Somerton, I.W., 1990. Magnetic interpretation in three dimensions using Euler deconvolution. Geophysics, 55(1): 80–91.
Ries, A.C., Shaekleton, R.M., Graham, R.H., and Fitches, W.R., 1983. Pan-African structures, ophiolites, and melange in the Eastern Desert of Egypt: A traverse at 26 degrees N. Journal of the Geological Society, London, 140: 75–95.
Sabet, A.H., EL Gaby, S., and Zalata, A.A., 1972. Geology of

the basement rocks in the northern parts of El Shayib and Safaga sheets, Eastern Desert. Annual Geological Survey, Egypt, 2: 111–128.
Sabins, F.F., 1999. Remote sensing for mineral exploration. Ore Geology Reviews, 14(3–4): 157–183.
Salem, A., Williams, S., Fairhead, J.D., Ravat, D., and Smith, R., 2007. Tilt-depth method: A simple depth estimation method using first-order magnetic derivatives. Lead Edge, 26(12): 1502–1505.
Serbouti, I., Raji, M., and Hakdaoui, M., 2022. Lithological mapping for a semi-arid area using GEOBIA and PBIA machine learning approaches with Sentinel-2 Imagery: Case study of Skhour Rehamna, Morocco. Advances in Science, Technology & Innovation, 143–156.
Shalaby, A., Stüwe, K., Makroum, F., Fritz, H., Kebede, T., and Klotzli, U., 2005. The Wadi Mubarak belt, Eastern Desert of Egypt: A neoproterozoic conjugate shear system in the Arabian–Nubian Shield. Precambrian Research, 136: 27–50.
Shebl, A., and Csámer, Á., 2021. Stacked vector multi-source lithologic classification utilizing machine learning algorithms: Data potentiality and dimensionality monitoring. Remote Sensing Applications: Society and Environment, 24: 100643.
Shebl, A., Abdellatif, M., Elkhateeb, S.O., and Csámer, Á., 2021. Multisource data analysis for gold potentiality mapping of Atalla area and its environs, central Eastern Desert, Egypt. Minerals, 11(6): 641.
Shebl, A., Kusky, T., and Csámer, Á., 2022. Advanced land imager superiority in lithological classification utilizing machine learning algorithms. Arabian Journal of Geosciences, 15: 923.
Stern, R.J., Johnson, P., Kröner, A., and Yibas, B., 2004. Neoproterozoic ophiolites of the Arabian–Nubian shield. In: Kusky, T.M. (ed.), Precambrian Ophiolites and Related Rocks. Amsterdam: Elsevier, 95–128.
Stern, R.J., 1994. Arc assembly and continental collision in the Neoproterozoic East African orogen: Implications for the consolidation of Gondwanaland. Annual Review of Earth and Planetary Sciences, 22: 319–351.
Surour, A.A., Attawiya, M.Y., Hussein, H.A., and El-Feky, M.G., 1999. Shear zone microfabrics and multiple sources of gold at the Hangaliya Mine, Eastern Desert, Egypt. Egypt. Journal of Geology, 43(1): 39–52.
Testa, F.J., Villanueva, C., Cooke, D.R., and Zhang, L., 2018. Lithological and hydrothermal alteration mapping of epithermal, porphyry and tourmaline breccia districts in the Argentine Andes using ASTER imagery. Remote Sensing, 10 (2): 203.
Thompson, D.T., 1982. EULDPH: A new technique for making computer assisted depth estimates from magnetic data. Geophysics, 47(1): 31–37.
Van der Meer, F.D., van der Werff, H.M.A., and van Ruitenbeek, F.J.A., 2014. Potential of ESA's Sentinel-2 for geological applications. Remote Sensing Applications: Society and Environment, 148: 124–133.
Volesky, J.C., Stern, R.J., and Johnson, P.R., 2003. Geological control of massive sulfide mineralization in the Neoproterozoic Wadi Bidah shear zone, southwestern Saudi Arabia, inferences from orbital remote sensing and field studies. Precambrian Research, 123(2–4): 235–247.
Yu, L., Porwal, A., Holden, E.J., and Dentith, M.C., 2012. Towards automatic lithological classification from remote sensing data using support vector machines. Computers & Geosciences, 45: 229–239.
Zoheir, B.A., Emam, A., El-Amawy, M., and Abu-Alam, T., 2017. Auriferous shear zones in the central Allaqi–Heiani belt: Orogenic gold in post-accretionary structures, SE Egypt. Journal of African Earth Sciences, 146: 118–131.
Zoheir, B.A., 2011. Transpressional zones in ophiolitic mélange terranes: Potential exploration targets for gold in the South Eastern Desert, Egypt. Journal of Geochemical Exploration, 111: 23–38.
Zoheir, B.A., and Akawy, A., 2010. Genesis of the Abu Marawat gold deposit, central Eastern Desert of Egypt. Journal of African Earth Sciences, 57: 306–320.
Zoheir, B.A., Steele-MacInnis, M., and Garbe-Schönberg, D., 2019. Orogenic gold formation in an evolving, decompressing hydrothermal system: Genesis of the Samut gold deposit, Eastern Desert, Egypt. Ore Geology Reviews, 105: 236–257.

About the first and corresponding author

Mohamed BADAWI, born in 1991 in Mansoura, Dakahliya Governorate, Egypt; master; graduated from Mansoura University; research assistant of Department of Geology, Faculty of Sciences, Mansoura University; Ph.D. candidate at Institute of Exploration Geosciences, University of Miskolc, Hungary. He is now interested in deformational features related to shear zones and their economic impact on hydrothermal alteration potentialities. E-mail: mohamedabdelhadi@mans.edu.eg.